J Polym Res (2016) 23: 43
DOI 10.1007/s10965-016-0937-1

ORIGINAL PAPER

High-density polyethylene/halloysite nanocomposites: morphology and rheological behaviour under extensional and shear flow

Vishwa Pratap Singh[1] · **K. K. Vimal**[2] · **G. S. Kapur**[2] · **Shashikant Sharma**[2] · **Veena Choudhary**[1]

Received: 25 August 2015 / Accepted: 5 February 2016 / Published online: 12 February 2016
© Springer Science+Business Media Dordrecht 2016

Abstract The paper describes the preparation of High Density Polyethylene [HDPE]/Halloysite Nanotube [HNT] nanocomposites by melt compounding HDPE with varying amounts of HNTs (ranging from 1 to 10 % *w/w*) in the absence and presence of MA-g-HDPE as compatibiliser using co-rotating twin screw extruder. The effect of HNT loading and compatibiliser amount on morphology and rheological properties was investigated. Melt strength and drawability were determined using Rheotens whereas extensional viscosity was calculated from (i) Wagner's master curve (using Rheotens data) and (ii) modified Cogswell method (using convergent flow analysis from capillary rheometer data). In HDPE/HNT composites, melt extensional properties (melt strength, drawability and extensional viscosity) increased slightly with increase in HNT concentration up to 5 % *w/w* followed by a decrease as HNT concentration was increased to 10 % *w/w*. On the other hand all these properties enhanced significantly in the presence of compatibiliser i.e. in HDPE/MA-g-HDPE/HNTs nanocomposites. Rheological studies form capillary rheometer showed marginal increase in the high shear viscosity at 10 % *w/w* filler loading. Both Complex viscosity and storage modulus in oscillatory rheometry were highest for nanocomposites prepared using 10 % *w/w* HNT and reduced slightly after incorporation of compatibiliser.

✉ Veena Choudhary
veenach@hotmail.com

[1] Centre for Polymer Science and Engineering, Indian Institute of Technology, New Delhi, India 110016

[2] Indian Oil Corporation Ltd. Research & Development Centre, Sector 13, Faridabad, Haryana, India 121007

Keywords HDPE · Halloysite nanotubes · HDPE-g-MA · Morphology · Rheology

Introduction

High Density Polyethylene (HDPE) is an important commodity thermoplastic, widely used in various applications due to its good mechanical properties, easy processability, recyclibility, good chemical resistance and biocompatibility at a relatively low cost. Properties of HDPE can be further improved by the incorporation of various inorganic or organic nanofillers into HDPE matrix [1]. HDPE based nanocomposites with various nanoparticles like carbon nanotubes (CNTs), nanoclays such as montmorillonite (MMT) and metal oxide nanoparticles have been widely reported in the literature [2–4]. However homogeneous dispersion of nanoparticles in polymer matrix has always been a challenge. In order to overcome the difficulty of poor phase adhesion between nanofillers and polymer, various strategies like surface modification of fillers and compatibilisers like standard polypropylene (PP) or polyethylene grafted with maleic anhydride (PP-g-MA or PE-g-MA) or polyethylene grafted with acrylic acid (PE-g-AA) have been studied by various researchers [5–9]. Minkova et al. [8] have investigated the influence of three different types of compatibilisers (ethylene-acrylic acid copolymer, acrylic acid grafted HDPE and maleic anhydride grafted HDPE) on the thermal properties of compatibilised HDPE/clay nanocomposites and correlated with the dispersion of clay [8]. Recently Mohamadi et al. explored the effect of molecular weight of HDPE-g-MA on the state of nanoclay dispersion in HDPE/fluoromica nanocomposites [10]. They reported better delamination of nanoclay layers in presence of low molecular weight HDPE-g-MA as compared to high

Table 1 Details of formulations and the designations of HDPE/HDPE-g-MA blends

Sample designation	HDPE (Weight %)	HDPE-g-MA (Weight %)
MAHD	–	100
HD/MAHD 5	95	5
HD/MAHD 10	90	10
HD/MAHD 15	85	15

HD represents HDPE; MAHD stands for HDPE-g-MA and numerical suffix represents weight percent of HDPE-g-MA

molecular weight compatibiliser due to the low viscosity and higher segmental mobility.

Halloysite is a kind of naturally occurring clay mineral with hollow micro and nanotubular morphology with typical dimensions i.e. inner diameter 15–100 nm, outer diameter 40–120 nm and length of 300–1000 nm [11] as shown in Fig. 2b. Halloysite nanotubes (HNT) are chemically similar to kaolinite ($Al_2[Si_2O_5(OH)_4].nH_2O$), where n is 2 and 0, indicating hydrated and dehydrated HNTs respectively [11]. It occurs in natural deposits of many countries like USA, France, New Zealand and China. Frost et al. [12] reported two types of hydroxyl groups, inner and outer hydroxyl groups, are situated between layers and on the surface of HNTs [12]. Because of its multilayer structure, most of the hydroxyl groups are situated on inner side and very few hydroxyl groups are located on the HNT surface. Consequently, dispersion of HNTs in the polymer matrix is easier as compared to other nanoparticles like carbon nanotubes, montmorillonite and fumed silica due to less intertubular contact and its rod like geometry [11]. The naturally occurring HNTs also have lower cost and are abundantly available as compared to carbon nanotubes (CNTs).

In recent years, polymeric nanocomposites containing HNTs as nanofiller have been a subject of research attention. HNTs can offer significant improvement in the thermal stability, fire resistance, mechanical properties and crystalline behaviour of polypropylene [13–17], linear low density polyethylene (LLDPE) [18], polyamide 6 (PA6) [19], epoxy resin [20], diene rubbers [21, 22], poly(lactic acid) [23, 24] etc. Although no surface modification/treatment of HNTs is required for the preparation of HNTs nanocomposites with highly polar polymers such as PA6 and epoxy resin having well distributed morphology. But in case of non-polar polyolefins such as PP, due to the discrepancy of polarity and chemical inertness of polyolefins, modification of HNTs [15, 25] as well as polymer [18, 26] is necessary to increase the compatibility between matrix and HNTs. Recently Liu et al. and Yuan et al. have reviewed the work on HNTs-polymer nanocomposites [27, 28]. Although lot of research has been carried out on the nanocomposites based on HNTs with various polymer matrices, but to the best of our knowledge HDPE/HNTs nanocomposites have not been reported in the literature.

Extensional behaviour of the polymers has a great importance in many polymer processings such as blow molding, melt spinning, film blowing and thermoforming where extensional deformation play an important role. Both shear and extensional flows are involved in these processing operations so there is a need for the characterization of these rheological properties of polymers in the presence of filler.

Over the years, the investigation of elongational flow properties for various homopolymers such as PP [29–31], low-density polyethylene (LDPE) [32] and HDPE [33] has been reported. Research in the extensional rheology area has also been extended from the homopolymers to polymer blends [34, 35] and filled polymers [36–38] that would provide enhanced physical, mechanical and processing properties. Garofalo et al. [39] investigated the uniaxial elongational flow properties of polyamide based nanocomposites by melt spinning which suggested that the addition of nanosilicate to polyamide could enhance drawdown force with decrease in the draw ratio at break. They described that the increase in drawdown force was caused by the increase of stiffness and elasticity in polymer nanocomposites. Su et al. [40] showed that the melt strength and elongational viscosity of nanoclay reinforced PP decreased with increasing nanoclay concentration up to 6 phr, however these properties improved slightly at higher filler

Table 2 Details of formulations and the designations of HDPE/HNT and HDPE/HDPE-g-MA/HNT nanocomposites

Sample Designation	HDPE (Weight %)	HNT (Weight %)	HDPE-g-MA (Weight %)	HNT: HDPE-g-MA
HD	100.0	0.0	–	
HDH 1	99	1.0	–	
HDH 3	97	3.0	–	
HDH 5	95	5.0	–	
HDH 10	90	10	–	
HDH 10/5C	85	10	5	1:0.5
HDH10/10C	80	10	10	1:1
HDH10/15C	75	10	15	1:1.5

Where HD represents HDPE, H stands for HNT and numerical suffix represents weight percent of HNTs, C represents compatibiliser numerical prefix represents weight percent of HDPE-g-MA

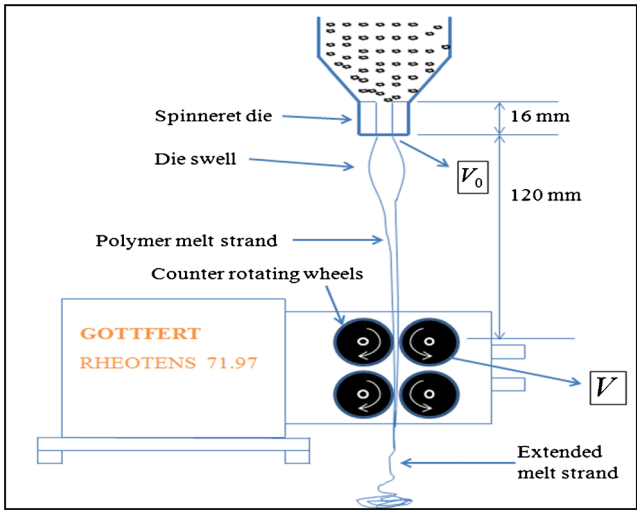

Fig. 1 Schematic diagram of Gottfert Rheotens melt strength tester setup for these studies

concentration. Kao et al. [37] investigated the extensional rheology of calcium carbonate ($CaCO_3$) filled PP over the concentration range of 0–43.8 vol% and found that the melt strength of $CaCO_3$-PP melts was independent of $CaCO_3$ content upto 25 vol% followed by a significant reduction of melt strength at higher concentration. Garcia et al. [38] used the convergent flow technique to determine the elongational viscosity of long glass fibre-filled HDPE and observed the increased elongational viscosity with increasing fibre content. McInerney et al. [41] measured the melt strength and extensibility of talc-filled PP by using Gottfert Rheotens^{TM} and claimed that the addition of talc to PP reduced melt strength as well as drawability. The decrease of melt strength was associated with the poor interaction between talc/PP interfaces.

As illustrated earlier, most studies in literature have been mainly focused on the study of elongational flow properties of polymers filled with glass fibers and inorganic fillers. Only very few articles have given attention to inorganic nanotubes (HNTs)/polymer composite melts [19]. Handge et al. [19] investigated the drawdown force of molten HNTs/PA6 composites using Rheotens apparatus. They suggested that increasing the HNT content in PA6/HNT nanocomposites resulted in a larger force and smaller drawability than neat PA6. They described that the decrease in drawability with addition of HNTs was caused by the percolation of neighboured nanotubes which leads to breakage of the strand.

The present work aims to incorporate HNTs into HDPE by melt mixing using masterbatch route and to investigate systematically the effect of HNTs and compatibilizer loading on morphology and rheological properties of nanocomposites. The main objective of this paper is to understand the correlation between HNTs dispersion and the resulting extensional and shear rheological properties.

Experimental section

Materials

HDPE (grade-012DB54, MFI = 1.2 g/10 min. at 190 °*C* and 5 kg load, density = 0.954 g/cm^3) was supplied by Indian Oil Corporation Ltd India. HNTs (BET surface area = 28 m^2/g) were purchased from Natural Nano Corp., USA and used as received. High density polyethylene grafted maleic anhydride (HDPE-g-MA) was used as a compatibiliser as it has some polar groups which are expected to enhance the interfacial adhesion with HNTs. It was available commercially (Optim E-156) from Pluss Polymers, Faridabad, India having following characteristics- MFI = 19.5 g/10 min. at 190 °C and 5 kg load, density = 0.953 g/cm3, MA content = 1 wt%. HDPE used in the present work is bimodal and has very low MFI (very high molecular weight). HDPE-g-MA having MFI higher as compared to HDPE was used to get better dispersion of filler as well as to enhance the adhesion between matrix and filler.

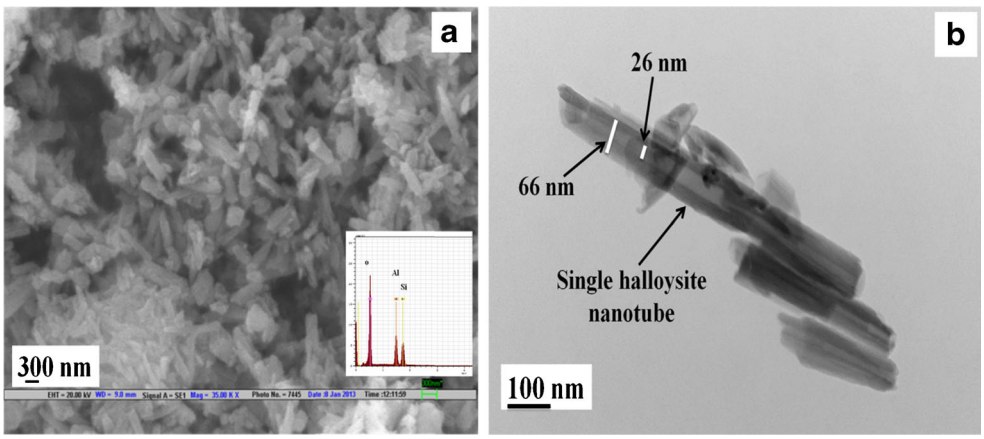

Fig. 2 (**a**) SEM image and (**b**) TEM image of HNTs

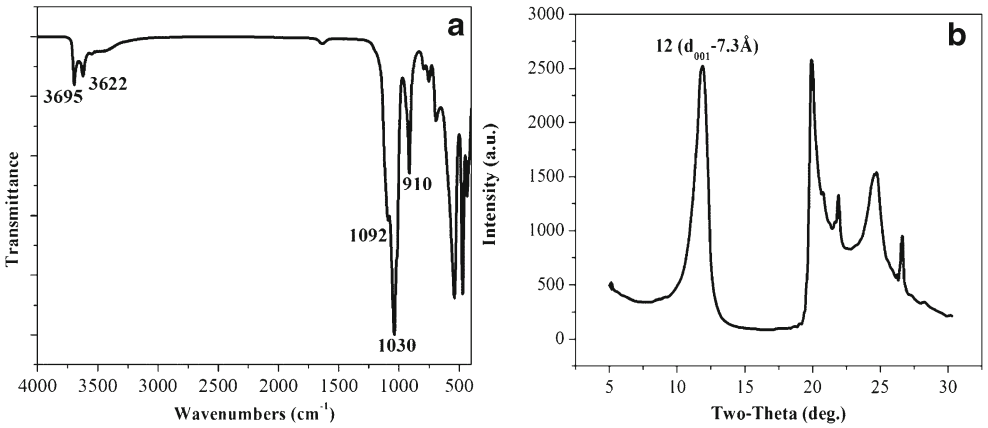

Fig. 3 (**a**) FTIR spectrum of HNTs and (**b**) XRD diffraction pattern of HNTs

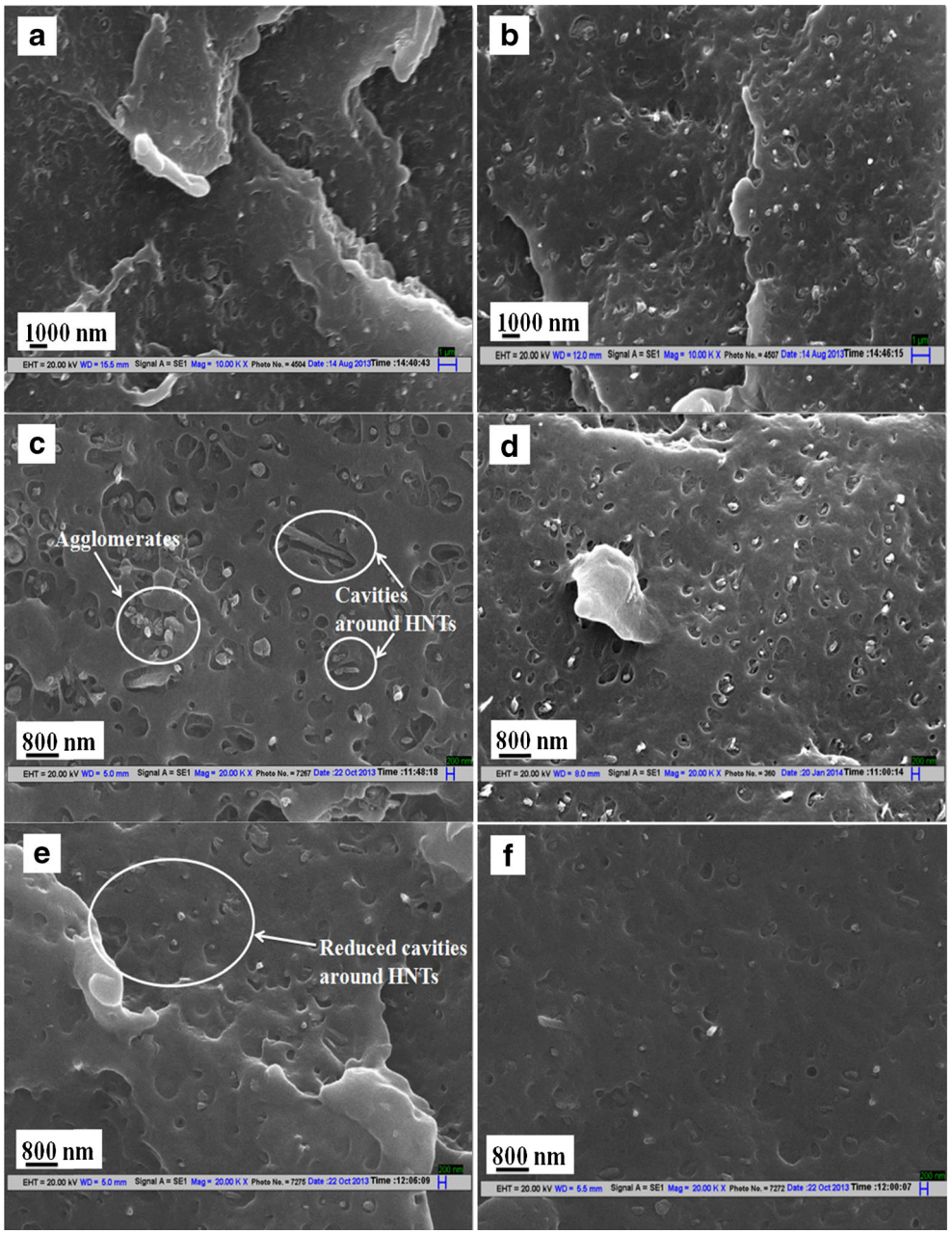

Fig. 4 SEM images of (**a**) HDH3, (**b**) HDH5, (**c**) HDH10, (**d**) HDH10/5C, (**e**) HDH10/10C and (f) HDH10/15C nanocomposites

Preparation of HDPE/HNT composites

HNT powder and polymer pellets (HDPE & HDPE-g-MA) were kept in vacuum oven at 80 °C for 24 h to remove absorbed moisture before mixing. HDPE/HNT nanocomposites were prepared in two steps i.e. (1) extrusion of a HDPE/HNT masterbatch containing 20 % *w/w* HNTs and (2) diluting this masterbatch with HDPE matrix to prepare different compositions of uncompatibilised and compatibilised nanocomposites. Blends based on HDPE/HDPE-g-MA were also prepared in order to study the influence of HDPE-g-MA on thermal, mechanical and rheological properties of HDPE. The details of formulations are given in Table 1 and Table 2. These compositions were compounded using a Lab. Tech. co-rotating twin screw extruder (L/D- 40 and screw diameter 25 mm). The temperature profile from the feed zone to die zone was 140 to 205 °C and screw speed was 100 rpm.

After compounding, test specimens were prepared using injection moulding machine (L&T- Demag PFY-40) at 205 °C keeping mould at 55 °C. Pristine HDPE was also subjected to extrusion in order to have the same thermal history.

Characterizations

Morphological characterization

Scanning electron microscopy (SEM) Morphological study was performed using SEM (EVO-50) on cryo-fractured surfaces of impact specimens at an acceleration voltage of 10 kV and under high vacuum. A thin layer of gold was sputter coated onto the fractured surface for 40s to avoid charging on exposure to electron beam during SEM analysis.

Transmission electron microscopy (TEM) Specimens were first microtomed into ultrathin sections (100 nm) by using an ultramicrotome (Power Tome-PC) from Boeckeler in liquid nitrogen. Then TEM analysis of the ultrathin samples was performed on a JEOL-JEM-2100 (LaB6) operated at an accelerating voltage of 100 kV.

Rheological characterizations

Rheotens test Rheotens measurement was carried out by using a four-wheeled Gottfert Rheotens 71.97 tester in

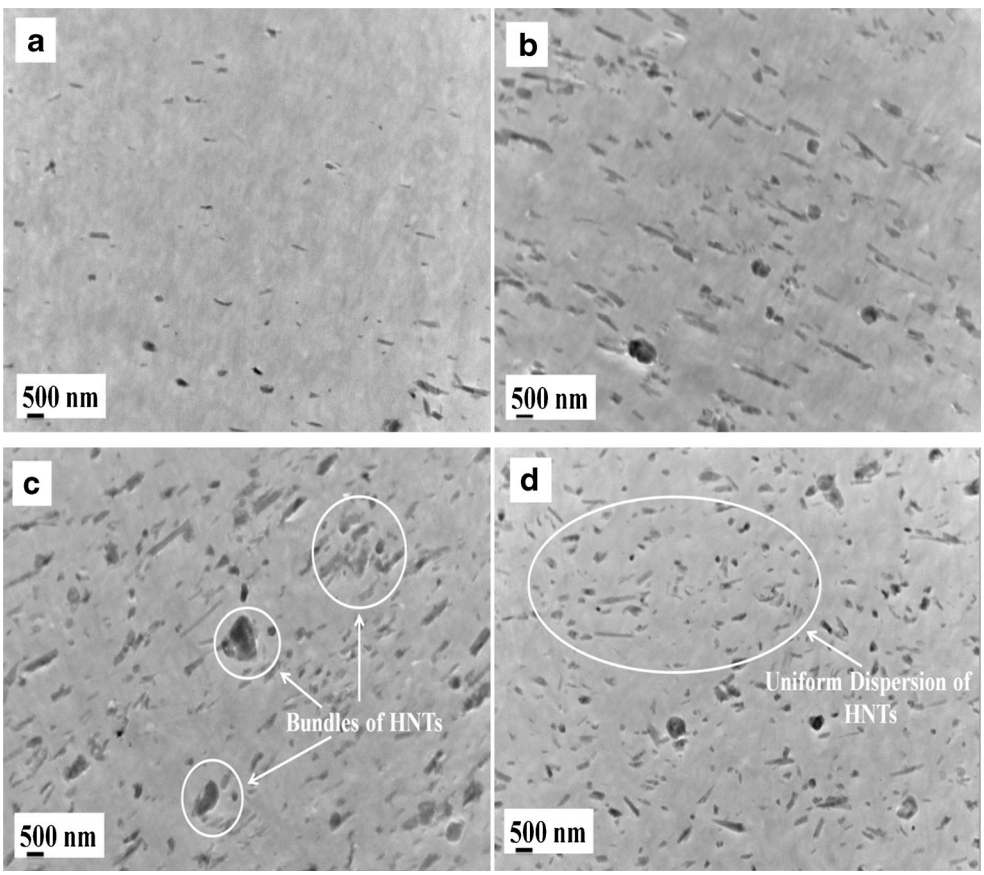

Fig. 5 TEM images of (**a**) HDH3, (**b**) HDH5, (**c**) HDH10 and (**d**) HDH10/15C nanocomposites

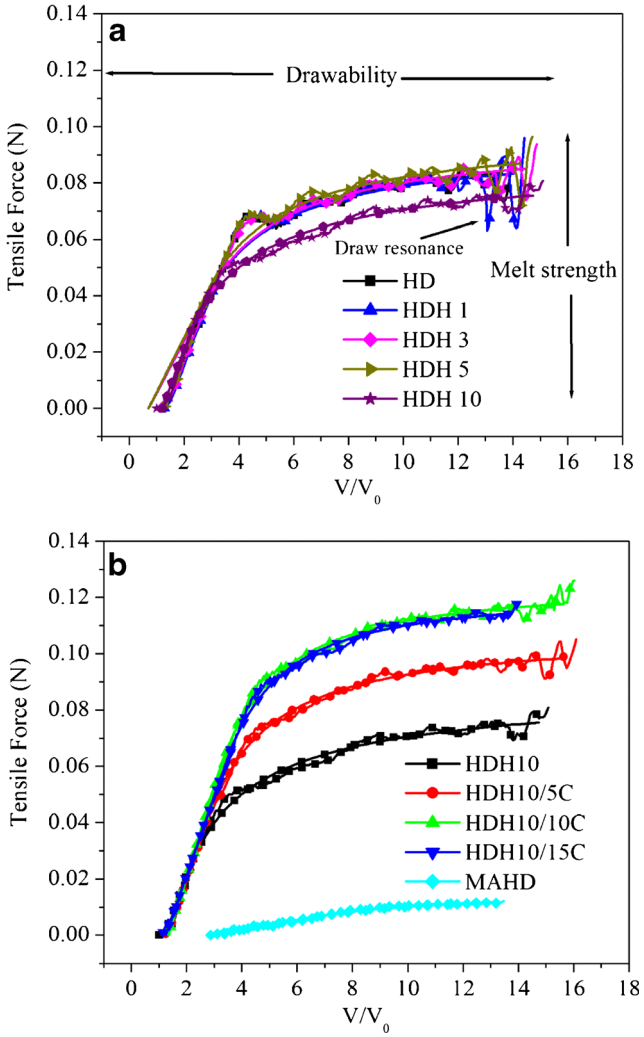

Fig. 6 Rheotens curves (Tensile force vs. draw down ratio) for neat HDPE and HDPE/HNT nanocomposites in absence (**a**)/presence (**b**) of compatibiliser at 200 °C

order to determine the melt strength and melt elongational properties of HDPE and its nanocomposites. A polymer melt strand was extruded from capillary die (L/D-15, D-2 mm) fitted in a capillary rheometer (Rosand RH7) with a constant output rate at 200 °C. This polymer melt strand was drawn by counter rotating rollers with increasing haul-off velocity at constant acceleration and the tensile force on the drawn melt strand was recorded. The tensile force and the velocity at the time of strand rupture are designated as melt strength and drawability of the polymer. A direct conversion of Rheotens diagram (tensile force versus draw down speed) into meaningful elongational viscosity versus elongational rate is not possible due to non-uniform strain rate imposed on the melt strand. Wagner et al. [42] offered a mathematical way to obtain Rheoten curves without oscillations.

The tensile stress at the wheels (σ), extensional rate ($\dot{\varepsilon}$) and extensional viscosity (η_e) were determined using the following equations.

$$\sigma = \frac{VF}{V_0 A_0} \tag{1}$$

$$\varepsilon = \frac{V}{Ls} \cdot \ln\left(\frac{V}{V_0}\right) \tag{2}$$

$$\eta_e = \frac{\sigma}{\dot{\varepsilon}} \tag{3}$$

Where F is force applied to the strand, V speed of wheels of Rheotens or speed at which strand is being pulled off, V_0 the filament extrusion velocity in the die, Ls the distance between the capillary exit and pinching wheels and A_0 diameter of strand. The schematic of experimental setup is shown in Fig. 1.

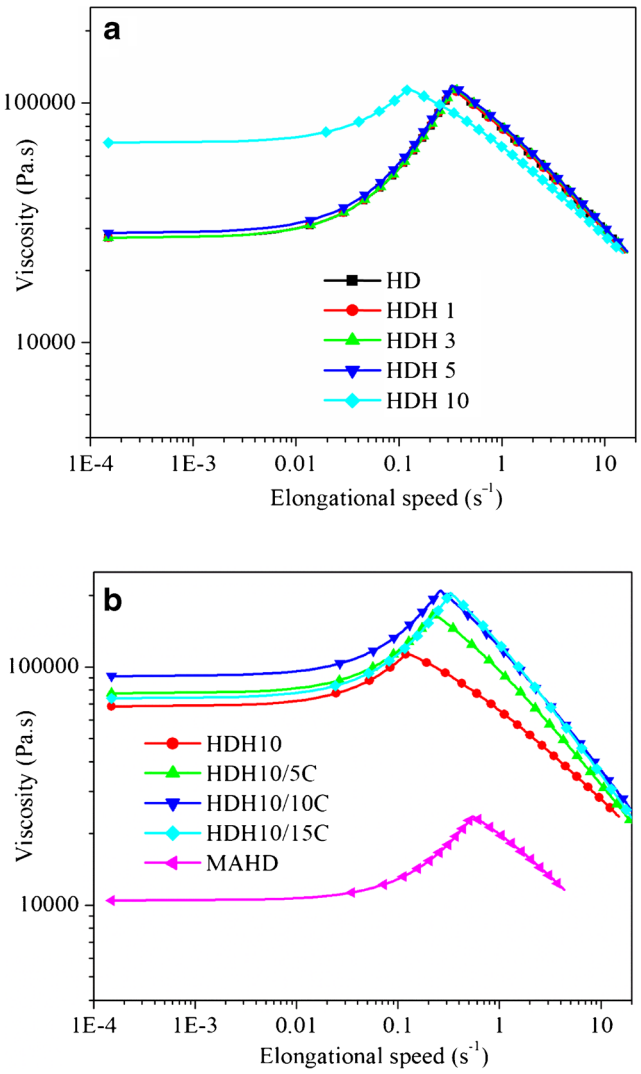

Fig. 7 Plots of extensional viscosity vs. extensional rate for neat HDPE and HDPE/HNT nanocomposites in absence (**a**)/presence (**b**) of compatibiliser [from standard Rheotens test] at 200 °C

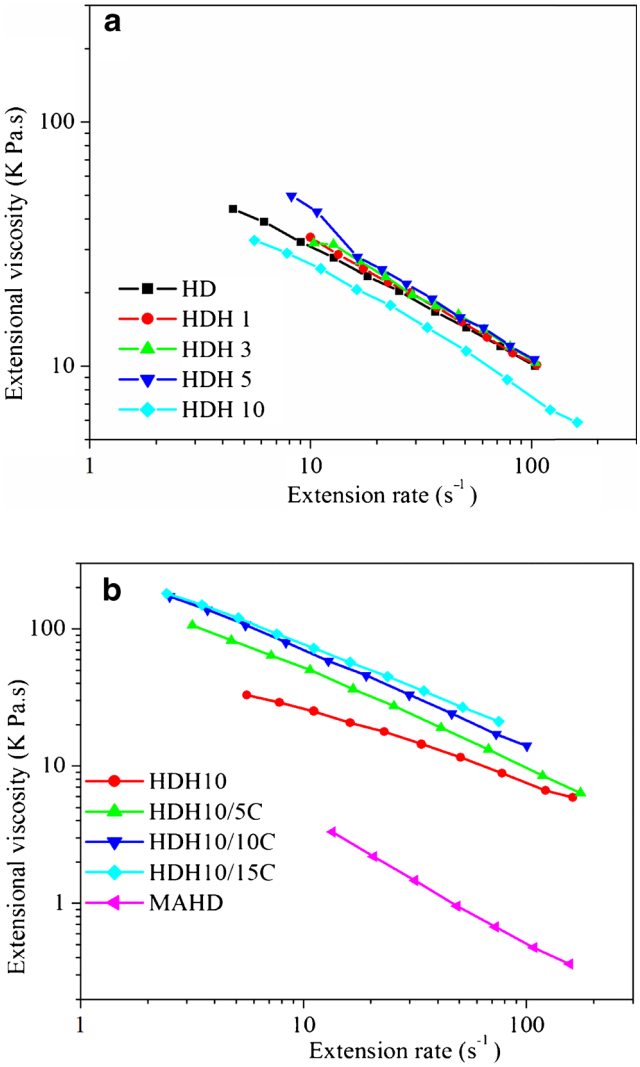

Fig. 8 Plots of extensional viscosity vs. extensional rate for neat HDPE and HDPE/HNT nanocomposites in absence (**a**)/presence (**b**) of compatibiliser [from capillary rheometer] at 200 °C

High shear rheology An advanced dual-bore (Bagley corrected) capillary rheometer, Rosand RH7 from Bohlin instruments was used to investigate the high shear viscosity and extensional viscosity of the HDPE and HDPE/HNT nanocomposites. The shear flow analysis was carried out using dual-bore having capillary die (L/D-16 mm, D-1 mm) in one bore and orifice die or zero length die in other bore. The shear rates ranging from 50 to 1000 s^{-1} at 200 °C were used during the steady shear experiment. Both Bagley and Rabinowitch corrected data were used for evaluation.

Cogswell converging flow method was used to calculate extensional viscosity from shear viscosity and die entrance pressure drop (ΔP) data at 200 °C. In this model it is assumed that the dependence of apparent shear viscosity (η_s) on the apparent shear rate is described by a power-law model and η_e is independent of $\dot{\varepsilon}$. Then η_e at the corresponding $\dot{\varepsilon}$ can be calculated as [43, 44]:

$$\eta_e = \left[\frac{3(n+1)\Delta P}{4\sqrt{2}\gamma_a}\right]^2 \frac{1}{\eta_s} \tag{4}$$

$$\varepsilon = \frac{\gamma_a}{2}\left(\frac{2\eta_s}{\eta_e}\right)^{1/2} \tag{5}$$

Where n is the power low index of the polymer melt.

Oscillatory rheometry The melt linear viscoelastic behaviour of HDPE and its nanocomposites was studied with ARES G2 rheometer equipped with 25 mm diameter parallel plates (gap-1.5 mm) in an oscillatory strain control mode. Dynamic frequency sweep experiments were performed at 190 °C over a frequency range of 0.0628–628 rad/s. Constant amplitude of 2 % was used to sustain the response of materials in the linear viscoelastic region.

Mechanical properties

Samples for mechanical properties were prepared using injection molding machine. Tensile tests were carried out according to ASTM D638 using a universal tensile testing

Table 3 Melt strength, drawability and slope in strain hardening region for HDPE and HDPE/HNT nanocomposites

Sample designation	Characteristics		
	Melt strength (N)	Drawability (mm/s)	Slope in strain hardening region*
HD	0.083	251	0.29
MAHD	0.012	242	0.04
HDH1	0.083	259	0.29
HDH3	0.085	267	0.28
HDH5	0.087	264	0.10
HDH10	0.075	272	0.15
HDH10/5C	0.098	289	0.17
HDH10/10C	0.12	288	0.20
HDH10/15C	0.11	251	0.29

*This characteristic was calculated from the extensional viscosity vs extensional speed curves of rheotens

machine (TIRA 2700) at room temperature. The crosshead speed was 50 mm/min. Flexural properties were evaluated using three point loading system on TIRA 2700 UTM as per ASTM D790 at a crosshead speed of 3 mm/min. Izod impact strength of the notched specimens was measured as per ASTM D256 by using CEAST impact tester. A notch of 2.54 mm depth with 45° was made on the specimen before testing. The average of five tests was considered and reported.

Thermal properties

The thermal stability of HDPE, HDPE/HDPE-g-MA blends, HDPE/HNT and HDPE/HDPE-g-MA/HNT composites was determined by recording thermogravimetric (TG) traces in air atmosphere using TGA-Q500 from TA instruments USA. The sample was heated from room temperature to 700 °C at a heating rate of 20 °C.

Results and discussion

Characterizations of HNTs

Morphological characterization of HNTs was done using SEM and TEM whereas structural and thermal characterizations were carried out using FTIR, XRD and TGA respectively.

SEM and TEM images of HNTs (Fig. 2a and b) show that the HNTs possess tubular shapes and some tubes are broken into shorter tubular particles. The average dimension of the individual tubes has inner diameter ranging from 15 to 100 nm, outer diameter in the range of 40–120 nm and length of 300–1000 nm with aspect ratio in the range of 35–100. The elemental composition of HNTs, determined by EDAX analysis consist of Al = 11.83 %, Si = 16.05 % and O = 72.12 %.

In the FTIR (Fig. 3a) spectrum of HNTs, the band at 3695 cm^{-1} confirms the presence of external hydroxyl groups while the absorption band at 3622 cm^{-1} is assigned to hydroxyl groups located on shared interfaces of layered structure consisting of silicon-oxygen tetrahedron and aluminium-oxygen octahedron. The absorption bands at 1092 and 1030 cm^{-1} belong to the stretching vibration of Si-O bonds. The characteristic absorption band at 910 cm^{-1} is assigned to flexural vibrations of Al-OH. The FTIR results confirm the co-existence of hydroxyl groups and Si-O bonds on the surface of HNTs. The XRD pattern of HNTs displays a characteristic reflection peak at 2 θ = 12° corresponding to basal spacing of 7.3 Å (Fig. 3b).

Thermal stability of HNTs was evaluated by recording thermogravimatric (TG) trace in air atmosphere (heating rate = 20 °C). HNTs showed a weight loss of 15.2 % in

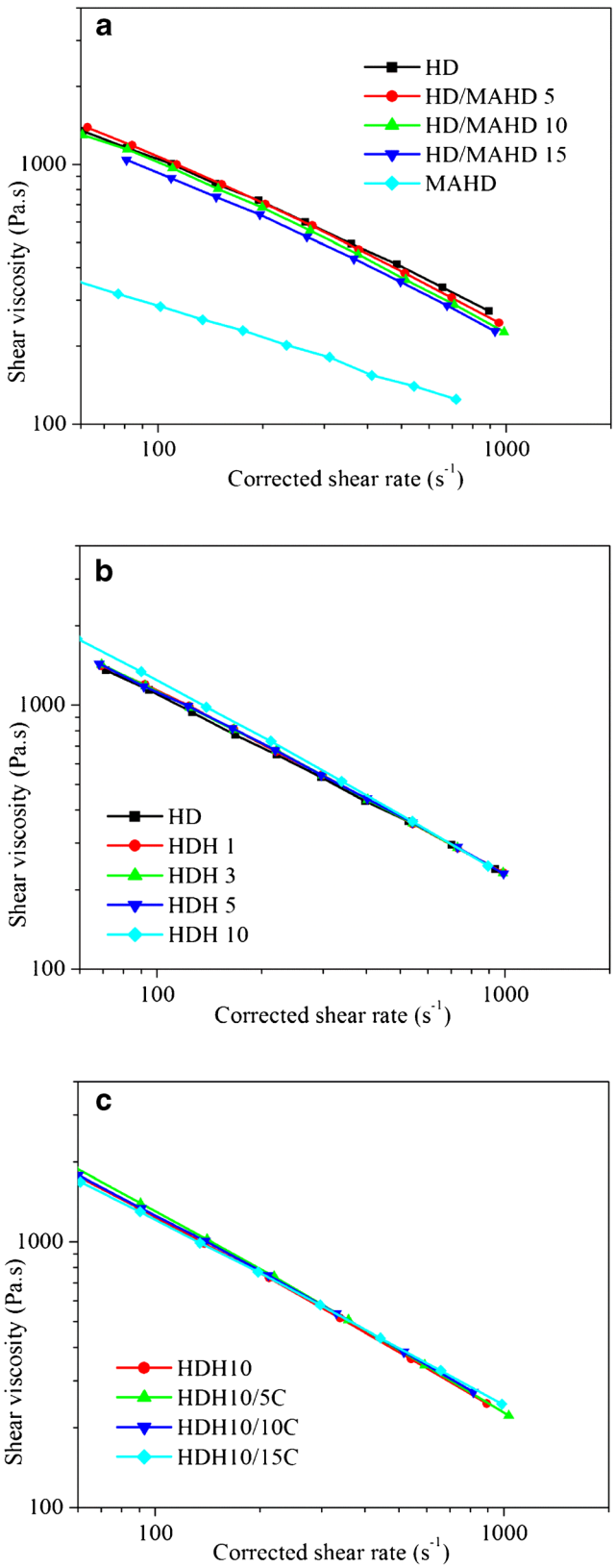

Fig. 9 Plots of shear viscosity vs. corrected shear rate for (**a**) HDPE, HDPE/HDPE-g-MA blends and their nanocomposites with HNTs in absence (**b**)/presence (**c**) of compatibiliser at 200 °C

temperature range of 420–520 °C which could be due to the loss of bound water.

Morphological characterizations of HDPE/HNT nanocomposites

Figure 4a-f shows the SEM images of cryogenically fractured surfaces of HDPE composites having varying amounts of HNTs. These micrographs illustrate the influence of HNTs loading as well as effect of compatibilizer (HDPE-g-MA) loading on the morphology. A uniform distribution of HNTs in the HDPE matrix was observed (Fig. 4a & b). This could be due to the lower density of hydroxyl groups on the surface of nanotubes, their tubular morphology and method used for compounding. However as the loading of HNTs was > 5 % *w/w*, formation of agglomerates and pull out of HNTs was seen (Fig. 4c). This could be due to the poor interaction between filler matrix which was improved significantly in the presence of compatibiliser (HDPE-g-MA) (Fig. 4d-f).

Morphological characterizations using TEM (Fig. 5b-d) also support the SEM results and confirm the existence of agglomerates of HNTs in the composites having higher loading of HNTs. However, aggregates are reduced or no more present in the compatibilized nanocomposites indicating better dispersion of HNTs in HDPE matrix in the presence of compatibiliser (Fig. 5e).

Rheological measurements

Melt strength and drawability

The average of five Rheotens measurements data plotted as tensile force versus draw down ratio (V/V_0) for HDPE and its nanocomposites (having varying concentrations of HNTs in

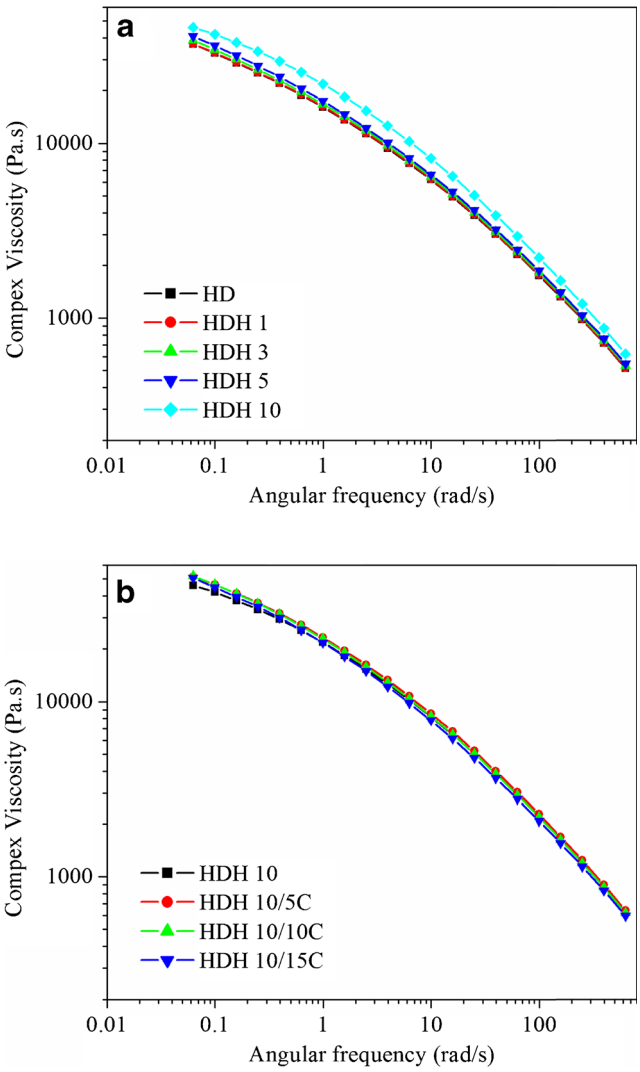

Fig. 10 Plots of complex viscosity *(η*)* vs. frequency of HDPE and HDPE/HNT nanocomposites in the absence (**a**)/presence (**b**) of compatibiliser at 190 °C

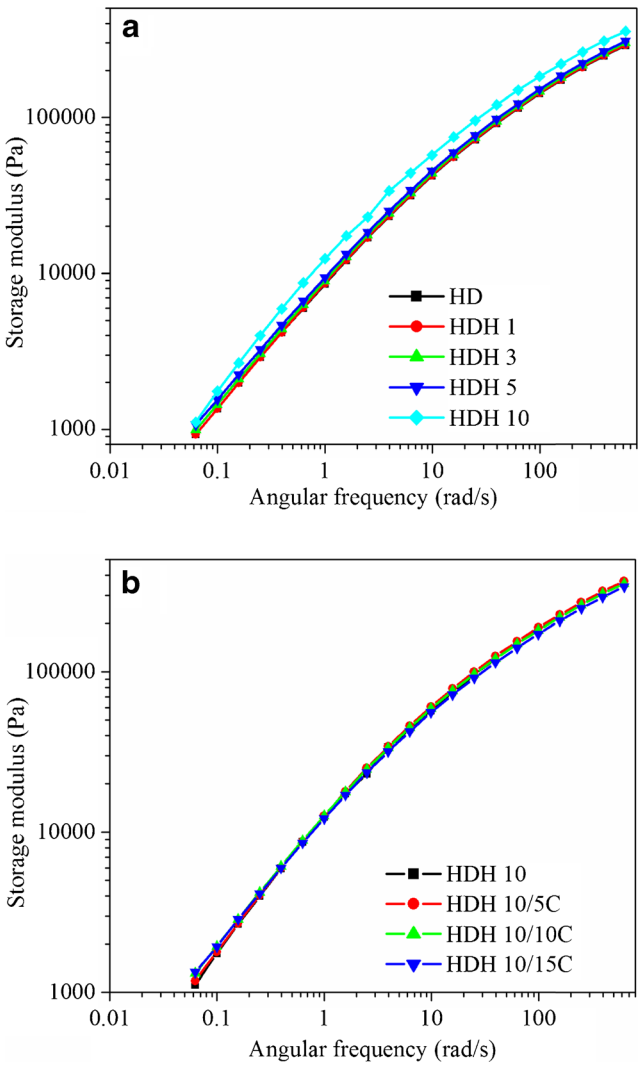

Fig. 11 Plots of storage modulus ***(G')*** vs. frequency for HDPE and HDPE/HNT nanocomposites in the absence (**a**)/presence (**b**) of compatibiliser at 190 °C

the absence/presence of compatibiliser) are shown in Fig. 6a and b. The point at which a molten polymer strand rupture indicates a relative measure for the melt strength and the drawability of the melt under test conditions [45].

All the nanocomposites (uncompatibilised & compatibilised) exhibited the filament rupture during testing. Interestingly, the drawability of the composites remains unaffected with increased HNT concentration upto 10 wt% whereas reduction in drawability of polymers has been reported in the presence of fillers [19, 37, 41, 46, 47]. The melt strength increased slightly upon incorporation of HNTs upto 5 % *w/w* followed by a decrease with increasing amount of HNTs. The reduction in melt strength at higher filler loading could be due to formation of agglomerates and voids which leads to the poor interaction between HDPE/HNT interface. This is also supported by the morphological characterization as observed by SEM & TEM. Figure 6b shows the Rheoten curves of compatibilised HDPE/HNT nanocomposites. It is clear from the graph that the tensile force as well as drawability increases significantly with the addition of compatibiliser to HDH10 composition (HDPE:HNT- 90:10) because HDPE-g-MA leads to adhesion enhancement between HDPE/HNT interfaces. This is also supported by the morphology of composites. It can be clearly depicted from Fig. 6b that the HDH10/10C composition shows a significant improvement of melt strength and drawability. At higher content of compatibiliser (HDH10/15C) a plasticizing effect was observed. In the previous studies, Lin et al. [46] have shown that higher elongational viscosity leads to higher melt strength and reduced drawability of the short glass fiber filled polypropylene. In the present studies i.e. HDPE/HNT and HDPE/HDPE-g-MA/HNTs, we observed that a higher elongational viscosity leads to higher melt strength without affecting drawability (Fig. 6a) or with increase in drawability (Fig. 6b) in case of HDPE/HDPE-g-MA/HNTs composites. Increase in the drawability of HDPE

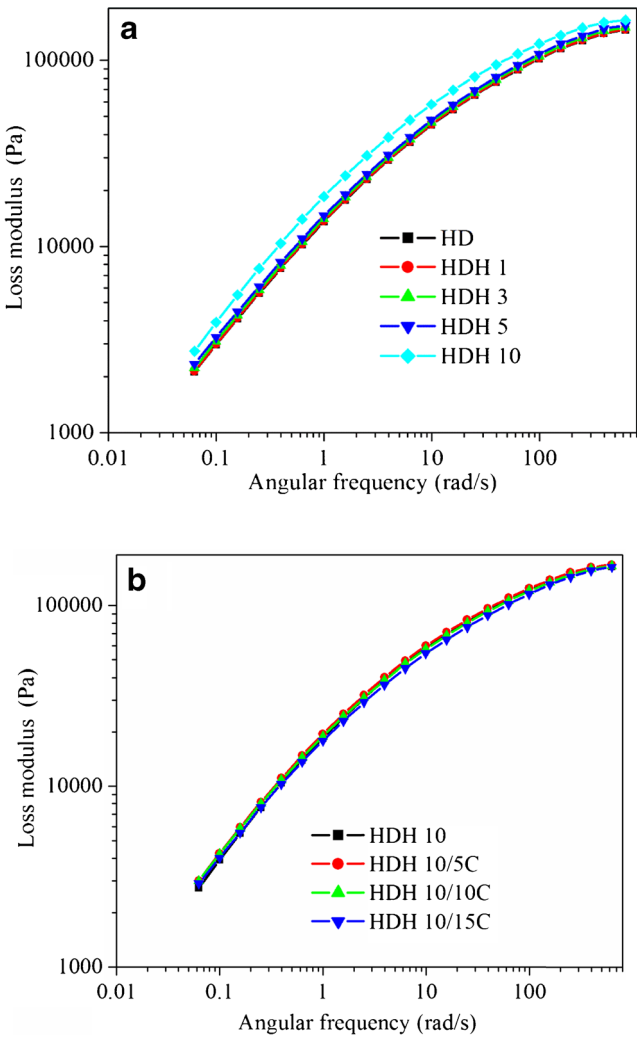

Fig. 12 Plots of Loss modulus ***(G")*** vs. frequency for HDPE and HDPE/HNT nanocomposites in the absence (**a**)/presence (**b**) of compatibiliser at 190 °C

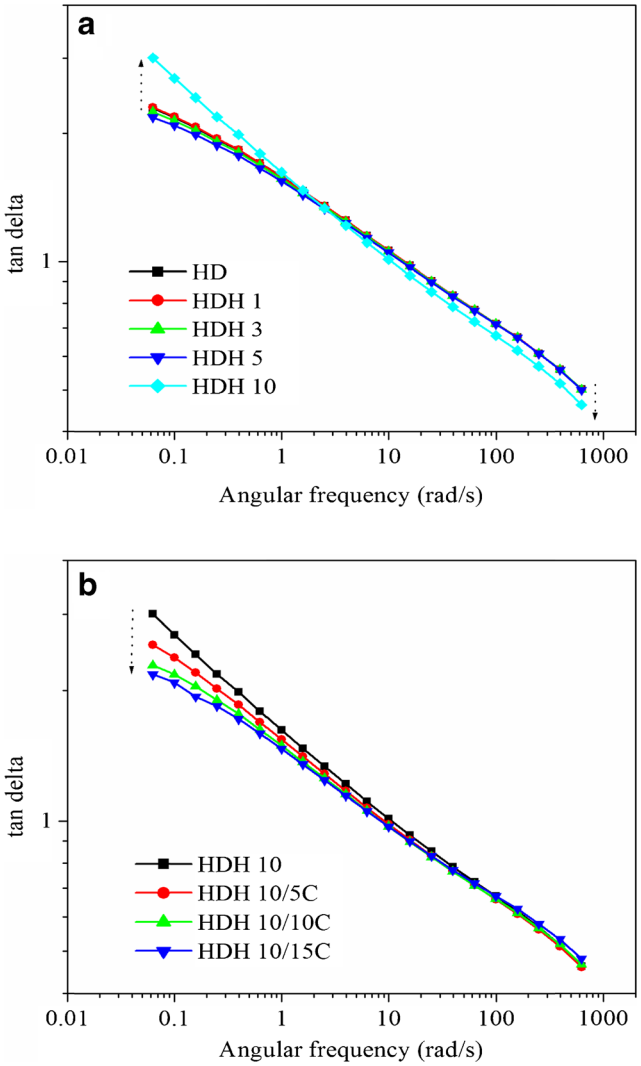

Fig. 13 Plots of tan δ vs. frequency for HDPE and HDPE/HNT nanocomposites in the absence (**a**)/presence (**b**) of compatibiliser at 190 °C

matrix upon incorporation of HNTs could be due to the better interfacial adhesion/dispersion of filler in HDPE matrix in presence of HDPE-g-MA. *This is an added advantage.*

Extensional viscosity

It is very important to understand the extensional rheology of molten polymers because it plays a significant role in polymer processing methods such as blow molding, film blowing, thermoforming and sheet casting etc. where stretching and drawing is involved at different stages.

The studies on η_e for HDPE and its nanocomposites was carried out using two different methods namely-

1. Performing Wagner's master curve using standard Rheotens data [42].

2. By Cogswell converging flow method using capillary data [43, 44].

Figures 7 & 8 shows the η_e versus extensional strain rate curves for uncompatibilised and compatibilised nanocomposites determined using Rheotens test and capillary rheometer respectively. Extensional viscosity increased with increase in HNT content up to 5 % *w/w* followed by a decrease with increase of HNT loading upto 10 % *w/w*. This reduction in η_e at higher filler loading could be due to the presence of some aggregates which could be reduced after incorporation of compatibiliser. This observation is supported by SEM/TEM images. Extensional viscosity (η_e) of HDPE/HNT (90/10, sample HDH10) enhanced significantly in the presence of 5 % *w/w* HDPE-g-MA as compatibiliser which showed an increase with increasing amounts of compatibiliser. This could be due to the improved adhesion between matrix and filler or due to the low molecular weight (higher MFI) of HDPE-g-MA. The main effects in the investigation of extensional

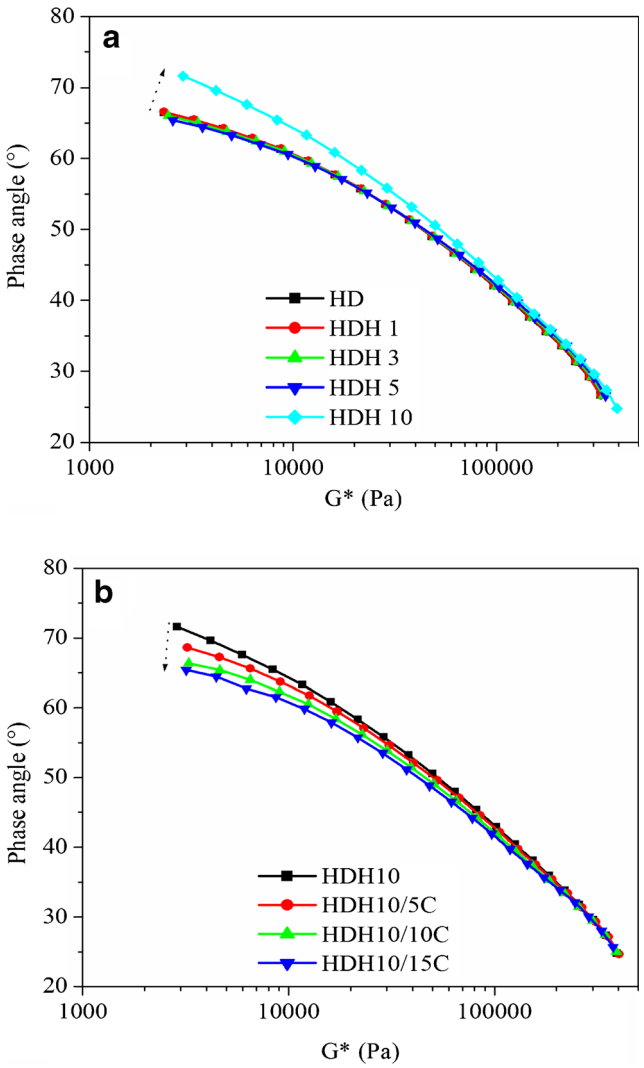

Fig. 14 van Grup-Palmen plots for HDPE and HDPE/HNT nanocomposites in the absence (**a**)/presence (**b**) of compatibiliser at 190 °C

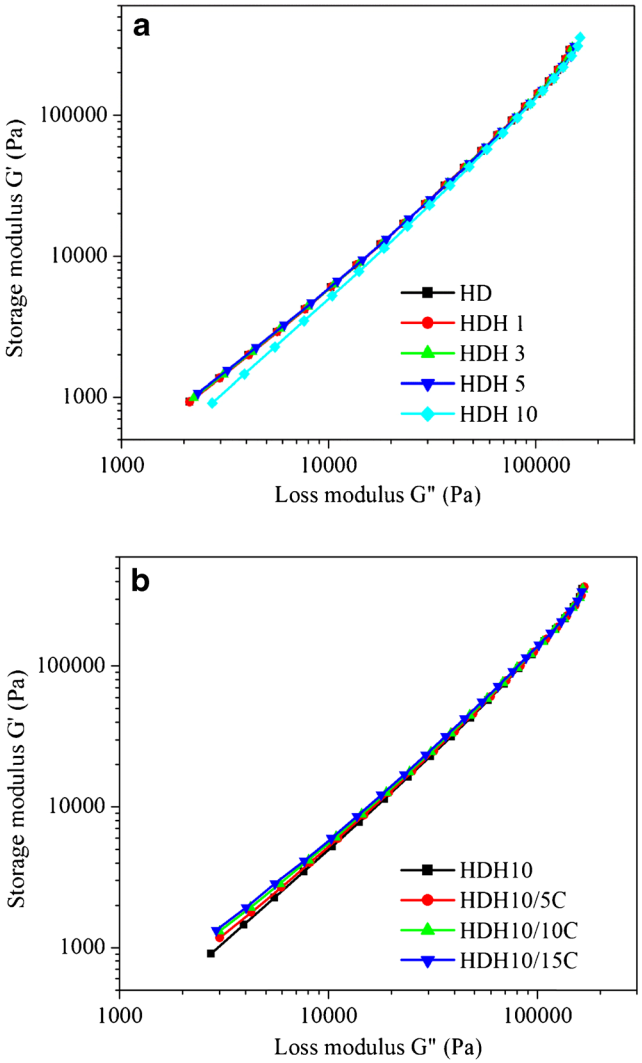

Fig. 15 Plots of ***G'*** vs. ***G"*** (Modified Cole-Cole plot) for HDPE and HDPE/HNT nanocomposites in the absence (**a**)/presence (**b**) of compatibiliser at 190 °C

viscosity and melt strength from Rheotens equipment are summarized in Table 3.

High shear rheology

Steady-state shear viscosity at 200 °C plotted against corrected shear rates are presented in Fig. 9a, b and c. The melt shear viscosities of all resins reduced with increasing the shear rate showing shear thinning and non-Newtonian flow behavior. It is evident from Fig. 9a that the shear viscosity of HDPE was found to be independent of HDPE-g-MA content upto 10 % *w/w* while slight reduction in shear viscosity was observed at 15 % *w/w* (sample-HD/MAHD 15) which may be due to the lower viscosity of compatibiliser.

The nanocomposites show some interesting results: the shear viscosity was found to be independent of the HNTs filler concentration up to 5 % *w/w*, after which it increased with further increase of filler concentration and HDH10 composition exhibits slight enhancement in melt shear viscosity only in the low shear rate region (Fig. 9b). This is beneficial from the processing point of view because processability of the filled and unfilled resins would be very similar over these concentration ranges. At high shear rate, viscosity of HDH 10 composition decreased because at higher shear rate, the presence of nanotubes in composites can slide with each other or orient themselves in the direction of flow and hence causing a flow-favouring orientation which subsequently lowers the viscosity of polymer matrix. As a consequence, reduction in the melt shear viscosities of nanocomposite resin was observed during their melt shear viscosity measurements. The nanocomposites prepared in the previous studies [48, 49] also exhibited similar shear thinning behaviour at higher shear rate. The shear viscosity was found to be independent of compatibiliser content over the range of 5–15 % *w/w* (Fig. 9c).

Oscillatory rheology

The variations in complex viscosity (η^*), storage modulus (G') and loss modulus (G'') as a function of angular frequency (ω) for neat HDPE and its nanocomposites are shown in Figs. 10, 11 and 12. It was observed that the complex viscosity of nanocomposites without compatibiliser (Fig. 10a) increases as the concentration of HNT increases in the low frequency region. At higher frequency (>10 rad/s), increase in viscosity is less pronounced and nanocomposites exhibit more shear thinning behaviour. This behaviour may occur due to the slipping between the polymer and filler at high shear rate or due to the orientation of nanotubes under high shear rate.

Addition of 5 and 10 wt% compatibiliser to HDH10 composition did not exhibit any significant effect on η*. Whereas sample containing 15 wt% compatibiliser showed more shear thinning behaviour at the frequency of more than 5 rad/s. This could be due to the low viscosity of compatibiliser (Fig. 10b). The curves of G' and G" for nanocomposites demonstrated a monotonic increase with increase in HNT content. No indication of a solid-like behaviour (plateau of G' and G" at low frequencies) can be observed upto 10 wt% HNTs (Figs. 11a and 12a). Although this behaviour was observed for other polymer nanocomposites [50–52] but there is no study in which somebody observed the pseudo-solid- like behaviour of polymer/HNT nanocomposites. This behaviour would be caused by the interaction among silicate particles that leads to apparent yield stress [53–55]. Handge et al. [19] determined the rheological properties of PA6/HNT nanocomposites and

Table 4 Mechanical testing data for neat HDPE, HDPE/ HDPE-g-MA blends, HDPE/HNT and HDPE/MAHD/HNT nanocomposites

Sample designation	Tensile strength (MPa)	Elongation at break (%)	Tensile modulus (MPa)	Flexural strength (MPa)	Flexural modulus (MPa)	Impact strength (KJ/m^2)
HD	27.5 ± 0.4	62 ± 4	293 ± 5.7	22.7 ± 0.2	760 ± 12	22.7 ± 1.5
MAHD	21.8 ± 1.0	217 ± 21	225 ± 11	19.2 ± 0.9	612 ± 16	3.3 ± 4.0
HDPE/MAHD blends						
HD/MAHD5	27.0 ± 0.6	67 ± 8	289 ± 6	22.3 ± 0.4	755 ± 5	21.6 ± 1.3
HD/MAHD10	26.3 ± 0.4	71 ± 6	276 ± 6	22.1 ± 0.6	739 ± 9	19.1 ± 0.9
HD/MAHD15	26.5 ± 0.3	81 ± 9	263 ± 8	21.8 ± 0.3	727 ± 10	16.8 ± 1.2
HDPE/HNT composites						
HDH1	27.1 ± 0.4	66 ± 6	291 ± 4.6	24.10 ± 0.2	805 ± 11	21.1 ± 0.4
HDH3	27.4 ± 0.2	63 ± 5	303 ± 2.3	25.4 ± 0.1	871 ± 7	18.7 ± 0.5
HDH5	27.3 ± 0.3	58 ± 3	312 ± 3.2	25.8 ± 0.2	890 ± 6	17.5 ± 0.6
HDH10	27.6 ± 0.2	50 ± 5	324 ± 2.5	26.1 ± 0.5	896 ± 12	15.6 ± 0.6
HDPE/MAHD/HNT composites						
HDH10/5C	28.8 ± 0.2	55 ± 6	318 ± 5.6	26.2 ± 0.2	898 ± 16	12.0 ± 0.4
HDH10/10C	29.2 ± 0.3	56 ± 7	319 ± 2.0	26.3 ± 0.2	887 ± 9	11.6 ± 0.3
HDH10/15C	29.0 ± 0.2	58 ± 9	312 ± 6.7	26.1 ± 0.4	881 ± 9	12.3 ± 0.7

indicated clearly that no evidence of pseudo-solid- like behaviour was observed in the composites even at the highest filler loading (30 wt%). In case of compatibilised systems, the storage and loss modulus both decreased when the amount of compatibiliser was raised from 5 to 15 wt% (Figs. 11b and 12b). This reduction in G' and G" observed in the presence of compatibiliser could be due to the low viscosity of HDPE-g-MA.

Tan δ is very sensitive to the structural changes of the material so the relationship between tan δ and frequency was also studied to investigate the damping characteristics of nanocomposites. It is evident that tan δ is independent of HNTs concentration upto 5 % *w/w* while sample having 10 % *w/w* of HNTs (i.e. sample HDH 10) showed quite different behaviour. Figure 13a show an increase in tan δ as HNTs loading increased to 10 % *w/w* particularly at lower frequency (<1 rad/s) and reduced continuously with increase in frequency. This behaviour in the low frequency region is an evidence for the presence of poor interfacial interactions between HDPE and HNTs as already discussed in morphological analysis. On the other hand, tan δ decrease with increasing addition of HD PE-g-MA contents in the nanocomposites as shown in Fig. 13b. The reduction in tan δ and hence the enhancement of interfacial bonding between the components indicate the dominance of G' over G", confirming that the composites become more elastic upon addition of HD PE-g-MA. This study is also in agreement with the previous study done by Mohsin et al. [56]. It is in line with the previous discussion about melt strength, drawability and extensional viscosity (Figs. 6, 7 and 8).

The morphology and the compatibility of two phase systems can also be studied by the van Grup-Palmen plot (Fig. 14) which presents the phase angle (δ)versus complex modulus (G*). From the van Grup-Palmen plot, it could be observed that HDPE and HDPE/HNT nanocomposites were predominantly viscous at terminal region as there is no curve with base line < 45° δ which was observed in case of HDPE-fumed silica nanocomposites and HDPE/UHMWPE blends in previous study [57, 58]. HDH 10 showed more viscous behaviour than other compositions (Fig. 14a). Another observation from the van Grup-Palmen plot is that with increase in HDPE-g-MA concentration (Fig. 14b), the phase angle of HDH 10 decreases and shifts towards lower value. This behaviour implies that the elastic response of HDPE/HNT nanocomposites increases after compatibilization. Similar results were also observed by Ezzati et al. [59].

Structural differences between the HDPE matrix and the nanocomposites was also confirmed by modified Cole-Cole plot i.e. by examining the relationship between *G'* vs. *G"*. Figure 15a and b shows the modified Cole-Cole plot of uncopatibilized and compatibilizied HDPE/HNTs nanocomposites. For the uncompatibilized HDPE/HNTs nanocomposites, the curves corresponding to 1–5 wt% of HNT content do not deviate from each other and from neat HDPE. But increase of HNT content to 10 wt% exhibits an increase in slope of *G'* vs. *G"* plot from other composition at lower frequency region indicating less interaction between filler and matrix (Fig. 15a). These poor interactions are caused by the formation of more aggregates and cavity, which induced heterogeneity within the composites. Unlike the uncompatibilized composites, when HDPE-g-MA was added to HDH 10 composition, decrease in the slope of *G'* vs. *G"* plot was observed over the range of 5–15 wt% of HDPE-g-MA content, indicating better compatibility between filler and matrix (Fig. 15b). Similar behaviour have been reported for HDPE-fumed silica composites [57].

Mechanical properties

The mechanical properties of composites mainly depend on factors such as the aspect ratio of filler, degree of dispersion of filler in the matrix, adhesion at the filler-matrix interface etc.

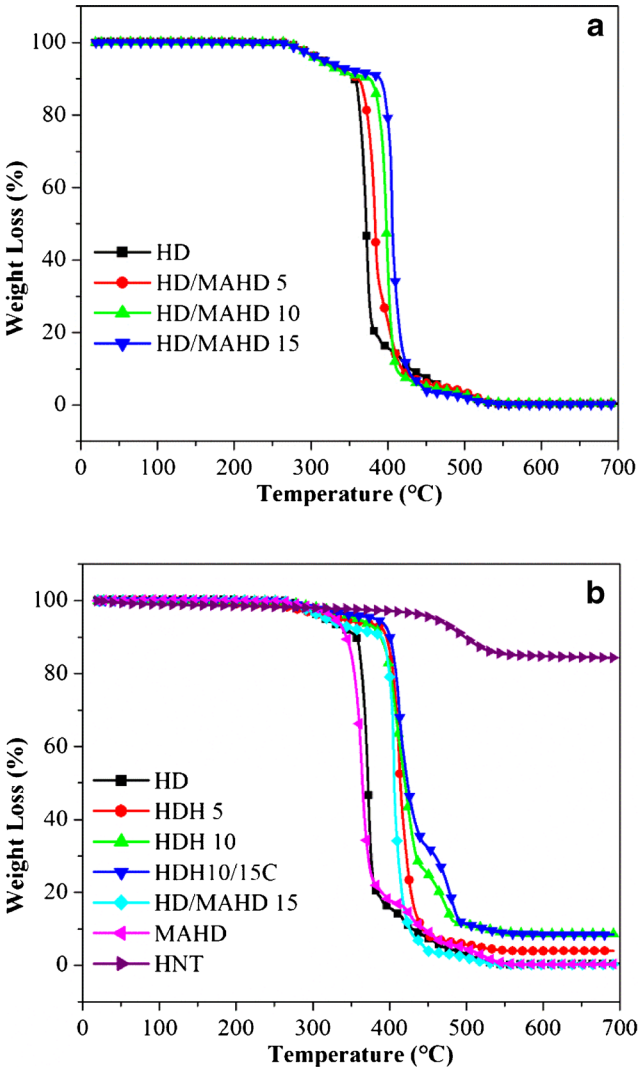

Fig. 16 TG traces of (**a**) HDPE, HDPE/HDPE-g-MA blends and (**b**) their nanocomposites with HNTs

The tensile and impact strength of HDPE-g-MA was lower as compared to HDPE (Table 4). Blending of HDPE with varying amounts of HDPE-g-MA did not affect tensile and flexural strength, however modulus and impact strength of HDPE decreased upon blending with HDPE-g-MA. The decrease in modulus could be due to the lower molecular weight of graft copolymer or due to its lower crystallinity.

Incorporation of HNTs up to 10 wt% did not affect the tensile properties. A marginal increase in tensile modulus was observed (~10 %) and it reduces upon the addition of compatibiliser but is always higher as compared to neat HDPE.

It appears that the addition of halloysite nanotubes leads to an improvement in flexural modulus and strength. The percent increase is about 17 % for flexural modulus and 12 % for flexural strength at 5 wt% HNT loading. While increasing the filler fraction from 5 to 10 wt% did not show any significant effect on flexural properties but modulus decreased slightly in compatibilised composites which show the plasticization effect of compatibiliser or likely due to the lower crystallinity of HDPE-g-MA compared to HDPE.

However it can be seen that the addition of halloysite nanotubes reduces the impact strength of nano- composites. The decrease in impact strength is due to the fact that the increase in the nanotube content leads to the formation of aggregates, which acts as stress concentrator in the sample, which initiate a brittle fracture. Even introduction of compatibiliser could not enhance the interfacial interaction between filler and matrix and further reduces the impact strength of matrix as the Izod impact strength for HDPE-g-MA was significantly lower than neat HDPE.

The incorporation of HNTs into a variety of polymer matrices act as reinforcing filler [18, 19, 25] however in case of PVDF, incorporation of HNTs resulted in a decrease in the mechanical properties because of large difference in the polarity of filler and matrix [27]. In case of PP, incorporation of HNTs did not change the tensile properties or improved slightly [16]. This was explained on the basis of nature of filler [HNTs] which has lower aspect ratio and thus did not show reinforcing effect. In the present work, we also observed that incorporation of HNTs in HDPE did not show much reinforcing effect as there is about 10 % increase in modulus without much change in tensile strength. Use of a compatibiliser helps in the dispersion of filler, inhibited the formation of aggregates but inspite of better adhesion/dispersion, properties deteriorated as HNTs have very low surface hydroxyl groups. The high shear forces generated during the processing of high molecular weight HDPE might have been responsible for the breakage of HNTs resulting in the formation of HNTs having lower aspect ratio and thus no reinforcement.

Thermal properties of HDPE, HDPE/HDPE-g-MA blends and their nanocomposites

Figure 16a and b shows the TG traces of HDPE/MAHD blends and HDPE/HNT nanocomposites. The thermal

Table 5 Results of thermogravimetric analysis for HDPE, HDPE/ HDPE-g-MA blends, HDPE/HNT and HDPE/ MAHD/HNT nanocomposites

Sample designation	$T_{0.1}$ (°C)	$T_{0.5}$ (°C)	% char at 700 (°C)		
			TGA	Muffle furnace	Theoretically calculated
HD	356	372	0.23	0.26	–
MAHD	344	365	0.3	0.26	–
HDPE/MAHD blends					
HD/MAHD 5	361	383	0.38	0.42	0.24
HD/MAHD 10	376	398	0.50	0.33	0.24
HD/MAHD 15	390	406	0.23	0.30	0.24
HDPE/HNT composites					
HDH 1	355	371	0.6	0.47	0.52
HDH 5	395	414	3.9	3.4	1.80
HDH 10	390	420	8.6	8.2	3.70
HDPE/MAHD/HNT composites					
HDH10/5C	404	419	8.7	7.8	3.59
HDH10/10C	405	418	8.4	8.6	3.63
HDH10/15C	401	424	8.4	7.7	3.63
HNT	498	–	84.2	83.4	–

stability was compared by comparing the degradation temperature at which 10 % mass loss occurs ($T_{0.1}$), the mid-point of degradation ($T_{0.5}$), and the nonvolatile residue found at 700 °C, denoted as char. These results of TG traces are summarized in Table 5. It can be seen that the decomposition temperatures of HD/MAHD blends and HD/HNT composites are higher than those of neat HDPE. In case of composites, it could be due to the hollow tubular structure and barrier effect of HNTs. The degradation products of HDPE may considerably be entrapped into the lumens of HNTs which delay in mass transport and enhance the thermal stability remarkably [14]. The thermal stability of HDH 10 composites further increases in the presence of compatibiliser. This could be due to the bonding of MA-g-HDPE on the surface of HNTs which might hinder the diffusion of volatiles and improve the dispersion of HNTs in the polymer matrix. As expected, the char yield increased with increasing amount of HNTs. From the knowledge of char yield of individual components, an attempt was made to calculate theoretical char yield using rule of mixtures according to the following equation:

$$\text{Char yield } (\%) = {}_{m}C_{m} + {}_{f}C_{f}$$

Where φ_m and φ_f are the volume fraction of matrix and filler in the nanocomposites and C_m and C_f are the char yield of matrix and filler, respectively. Theoretical values are lower as compared to experimental values. This could be due to the hindrance of evolution of volatile products in the presence of HNTs due to its well known barrier effect. Percent char yield in HNTs, HDPE, HD/HNT nanocomposites and HD/MAHD blends was also obtained from muffle furnace according to ASTM 5630–13. It was observed that there is a very good agreement in the values of char yield obtained from TG traces and muffle furnace (Table 5).

Conclusions

From these studies following conclusions can be drawn.

(1) Incorporation HDPE-g-MA as compatibiliser improved the dispersion of HNTs and interfacial adhesion between matrix and filler.
(2) Melt extensional properties (Extensional viscosity & Melt strength) enhanced significantly in the presence of compatibiliser. Optimum amount of compatibiliser was found to be 1:1 i.e. filler: compatibiliser.
(3) Extensional viscosity calculated using two different methods (Cogswell converging flow method & Wagner's master curve) exhibited good agreement.
(4) Viscosity decreased slightly in the presence of compatibiliser.
(5) The lower viscosity observed in HD/HDPE-g-MA/HNT composites could be due to the lower viscosity of the compatibiliser or due to the alignment of tubes in the direction of flow and not due to the degradation as all the materials were stable at 200 °C.
(6) Though a good dispersion of HNTs in HDPE matrix was observed, improvement in mechanical properties was marginal.
(7) Such composites can be used for processing like blow moulding, film blowing and sheet casting.

Acknowledgments The authors thank Ministry of Human Resource Development (MHRD), India for providing financial assistance to one of the authors Mr. Vishwa Pratap Singh. The authors also thank the Director IOCL R&D center for providing the characterization facilities.

References

1. Ahmad AA, Al-Juhani AA, Thomas S, De SK, Atieh MA (2013) Effect of modified and nonmodified carbon nanotubes on the rheological behavior of high density polyethylene nanocomposite. J Nanomater 2013:12. doi:10.1155/2013/731860
2. Osman MA, Atallah A (2006) Effect of the particle size on the viscoelastic properties of filled polyethylene. Polymer 47(7): 2357–2368. doi:10.1016/j.polymer.2006.01.085
3. Tang Y, Yang C, Gao P, Ye L, Zhao C, Lin W (2011) Rheological study on high-density polyethylene/organoclay composites. Polym Eng Sci 51(1):133–142. doi:10.1002/pen.21790
4. Vega JF, Martínez-Salazar J, Trujillo M, Arnal ML, Müller AJ, Bredeau S, Dubois P (2009) Rheology, processing, tensile properties, and crystallization of polyethylene/carbon nanotube nanocomposites. Macromolecules 42(13):4719–4727. doi:10.1021/ma900645f
5. Zhong Y, De Kee D (2005) Morphology and properties of layered silicate-polyethylene nanocomposite blown films. Polym Eng Sci 45(4):469–477. doi:10.1002/pen.20306
6. Durmuş A, Woo M, Kaşgöz A, Macosko CW, Tsapatsis M (2007) Intercalated linear low density polyethylene (LLDPE)/clay nanocomposites prepared with oxidized polyethylene as a new type compatibilizer: Structural, mechanical and barrier properties. Eur Polym J 43(9):3737–3749. doi:10.1016/j.eurpolymj.2007.06.019
7. Xu Y, Fang Z, Tong L (2005) On promoting intercalation and exfoliation of bentonite in high-density polyethylene by grafting acrylic acid. J Appl Polym Sci 96(6):2429–2434. doi:10.1002/app.21708
8. Minkova L, Peneva Y, Tashev E, Filippi S, Pracella M, Magagnini P (2009) Thermal properties and microhardness of HDPE/clay nanocomposites compatibilized by different functionalized polyethylenes. Polym Test 28(5):528–533. doi:10.1016/j.polymertesting.2009.04.001
9. Picard E, Vermogen A, Gérard JF, Espuche E (2008) Influence of the compatibilizer polarity and molar mass on the morphology and the gas barrier properties of polyethylene/clay nanocomposites. J Polym Sci B Polym Phys 46(23):2593–2604. doi:10.1002/polb.21584
10. Mohamadi M, Garmabi H, Keshavarzi F (2014) Structural characterization of high-density polyethylene nanocomposites: effect of compatibilizer type and high aspect ratio organoclay platelets. Polym Bull 71(10):2709–2731. doi:10.1007/s00289-014-1219-x

11. Du M, Guo B, Jia D (2010) Newly emerging applications of halloysite nanotubes: a review. Polym Int 59(5):574–582. doi:10.1002/pi.2754
12. Frost RL, Shurvell HF (1997) Raman microprobe spectroscopy of halloysite. Clay Clay Miner 45(1):68–72
13. Du M, Guo B, Wan J, Zou Q, Jia D (2010) Effects of halloysite nanotubes on kinetics and activation energy of non-isothermal crystallization of polypropylene. J Polym Res 17(1):109–118. doi:10.1007/s10965-009-9296-5
14. Du M, Guo B, Jia D (2006) Thermal stability and flame retardant effects of halloysite nanotubes on poly(propylene). Eur Polym J 42(6):1362–1369. doi:10.1016/j.eurpolymj.2005.12.006
15. Lecouvet B, Sclavons M, Bourbigot S, Devaux J, Bailly C (2011) Water-assisted extrusion as a novel processing route to prepare polypropylene/halloysite nanotube nanocomposites: structure and properties. Polymer 52(19):4284–4295. doi:10.1016/j.polymer.2011.07.021
16. Ning N-y, Q-j Y, Luo F, Zhang Q, Du R, Fu Q (2007) Crystallization behavior and mechanical properties of polypropylene/halloysite composites. Polymer 48(25):7374–7384. doi:10.1016/j.polymer.2007.10.005
17. Lecouvet B, Bourbigot S, Sclavons M, Bailly C (2012) Kinetics of the thermal and thermo-oxidative degradation of polypropylene/halloysite nanocomposites. Polym Degrad Stab 97(9):1745–1754. doi:10.1016/j.polymdegradstab.2012.06.022
18. Jia Z, Luo Y, Guo B, Yang B, Du M, Jia D (2009) Reinforcing and flame-retardant effects of halloysite nanotubes on LLDPE. Polymer-Plastics Technol Eng 48(6):607–613. doi:10.1080/03602550902824440
19. Handge UA, Hedicke-Höchstötter K, Altstädt V (2010) Composites of polyamide 6 and silicate nanotubes of the mineral halloysite: influence of molecular weight on thermal, mechanical and rheological properties. Polymer 51(12):2690–2699. doi:10.1016/j.polymer.2010.04.041
20. Liu M, Guo B, Du M, Cai X, Jia D (2007) Properties of halloysite nanotube–epoxy resin hybrids and the interfacial reactions in the systems. Nanotechnology 18(45):455703
21. Rybiński P, Janowska G, Jóźwiak M, Pająk A (2012) Thermal properties and flammability of nanocomposites based on diene rubbers and naturally occurring and activated halloysite nanotubes. J Therm Anal Calorim 107(3):1243–1249. doi:10.1007/s10973-011-1787-z
22. Rybiński P, Janowska G (2013) Influence synergetic effect of halloysite nanotubes and halogen-free flame-retardants on properties nitrile rubber composites. Thermochim Acta 557:24–30. doi:10.1016/j.tca.2013.01.030
23. Liu M, Zhang Y, Zhou C (2013) Nanocomposites of halloysite and polylactide. Appl Clay Sci 75–76:52–59. doi:10.1016/j.clay.2013.02.019
24. Prashantha K, Lecouvet B, Sclavons M, Lacrampe MF, Krawczak P (2013) Poly(lactic acid)/halloysite nanotubes nanocomposites: structure, thermal, and mechanical properties as a function of halloysite treatment. J Appl Polym Sci 128(3):1895–1903. doi:10.1002/app.38358
25. Prashantha K, Lacrampe M, Krawczak P (2011) Processing and characterization of halloysite nanotubes filled polypropylene nanocomposites based on a masterbatch route: effect of halloysites treatment on structural and mechanical properties. Express Polymer Lett 5(4):295–307
26. Khunova V, Kristof J, Kelnar I et al. (2013) The effect of halloysite modification combined with in situ matrix modifications on the structure and properties of polypropylene/halloysite nanocomposites. Express Polymer Lett 7 (5)
27. Liu M, Jia Z, Jia D, Zhou C (2014) Recent advance in research on halloysite nanotubes-polymer nanocomposite. Prog Polym Sci 39(8):1498–1525. doi:10.1016/j.progpolymsci.2014.04.004
28. Yuan P, Tan D, Annabi-Bergaya F (2015) Properties and applications of halloysite nanotubes: recent research advances and future prospects. Appl Clay Sci 112–113:75–93. doi:10.1016/j.clay.2015.05.001
29. Ghijsels A, De Clippeleir J (1994) Melt strength behaviour of polypropylenes. Int Polym Process 9(3):252–257. doi:10.3139/217.940252
30. Lau HC, Bhattacharya SN, Field GJ (1998) Melt strength of polypropylene: its relevance to thermoforming. Polym Eng Sci 38(11):1915–1923. doi:10.1002/pen.10362
31. Muke S, Ivanov I, Kao N, Bhattacharya SN (2001) The melt extensibility of polypropylene. Polym Int 50(5):515–523. doi:10.1002/pi.654
32. Sampers J, Leblans PJR (1988) An experimental and theoretical study of the effect of the elongational history on the dynamics of isothermal melt spinning. J Non-Newtonian Fluid Mech 30(2–3):325–342. doi:10.1016/0377-0257(88)85032-8
33. Lacaze JM, Marin G, Monge P (1988) Elongational rheology of polyethylene melts—temporary network constitutive laws. Rheol Acta 27(5):540–545. doi:10.1007/bf01329354
34. Micic P, Bhattacharya SN, Field G (1997) Rheological behaviour of LLDPE/LDPE blends under elongational deformation. Int Polym Process 12(2):110–115. doi:10.3139/217.970110
35. Field GJ, Micic P, Bhattacharya SN (1999) Melt strength and film bubble instability of LLDPE/LDPE blends. Polym Int 48(6):461–466. doi:10.1002/(sici)1097-0126(199906)48:6<461::aid-pi169>3.0.co;2-7
36. Kobayashi M, Takahashi T, Takimoto J-i, Koyama K (1996) Influence of glass beads on the elongational viscosity of polyethylene with anomalous strain rate dependence of the strain-hardening. Polymer 37(16):3745–3747. doi:10.1016/0032-3861(96)00191-7
37. Kao N, Chandra A, Bhattacharya S (2002) Melt strength of calcium carbonate filled polypropylene melts. Polym Int 51(12):1385–1389. doi:10.1002/pi.1057
38. Garcia-Rejon A, Meddad A, Turcott E, Carmel M (2002) Extrusion blow molding of long fiber reinforced polyolefins. Polym Eng Sci 42(2):346–364. doi:10.1002/pen.10953
39. Garofalo E, Russo GM, Di Maio L, Incarnato L (2007) Study on the effect of uniaxial elongational flow on polyamide based nanocomposites. Macromol Symp 247(1):110–119. doi:10.1002/masy.200750113
40. Su F-H, Yan J-H, Huang H-X (2011) Structure and melt rheology of long-chain branching polypropylene/clay nanocomposites. J Appl Polym Sci 119(2):1230–1238. doi:10.1002/app.32800
41. McInerney LF, Kao N, Bhattacharya SN (2003) Melt strength and extensibility of talc-filled polypropylene. Polym Eng Sci 43(12):1821–1829. doi:10.1002/pen.10154
42. Wagner MH, Bernnat A, Schulze V (1998) The rheology of the rheotens test. J Rheol (1978-present) 42(4):917–928. doi:10.1122/1.550907
43. Cogswell FN (1972) Measuring the extensional rheology of polymer melts. Trans Soc Rheol (1957–1977) 16(3):383–403. doi:10.1122/1.549257
44. Wang Q-J, Huang H-X (2013) Detecting extensional viscosity of polypropylene melt using the Rheotens test: a comparison between standard and steady state test modes. Polym Test 32(8):1400–1407. doi:10.1016/j.polymertesting.2013.09.001
45. Wang KH, Xu M, Choi YS, Chung IJ (2001) Effect of aspect ratio of clay on melt extensional process of maleated polyethylene/clay nanocomposites. Polym Bull 46(6):499–505. doi:10.1007/s002890170038
46. Lin G-G, Hu M-C (1997) Measurement of elongation viscosity for polymer melts by fiber spinning. Adv Polym Technol 16(3):199–207. doi:10.1002/(sici)1098-2329(199723)16:3<199::aid-adv4>3.0.co;2-o

47. Koo CM, Kim JH, Wang KH, Chung IJ (2005) Melt-extensional properties and orientation behaviors of polypropylene-layered silicate nanocomposites. J Polym Sci B Polym Phys 43(2):158–167. doi:10.1002/polb.10564
48. Yeh J-T, Yao W-H, Chen C-C (2005) Polar and non-polar solvent permeation resistance of blow-molded bottles of polyethylene/blends of modified polyamide and polyamide 6 clay nanocomposite. J Polym Res 12(4):279–287. doi:10.1007/s10965-004-5480-9
49. Cho JW, Paul DR (2001) Nylon 6 nanocomposites by melt compounding. Polymer 42(3):1083–1094. doi:10.1016/S0032-3861(00)00380-3
50. McNally T, Pötschke P, Halley P, Murphy M, Martin D, Bell SEJ, Brennan GP, Bein D, Lemoine P, Quinn JP (2005) Polyethylene multiwalled carbon nanotube composites. Polymer 46(19):8222–8232. doi:10.1016/j.polymer.2005.06.094
51. Krishnamoorti R, Giannelis EP (1997) Rheology of end-tethered polymer layered silicate nanocomposites. Macromolecules 30(14):4097–4102. doi:10.1021/ma960550a
52. Lee YH, Park CB, Wang KH, Lee MH (2005) HDPE-clay nanocomposite foams blown with supercritical CO2. J Cell Plast 41(5):487–502. doi:10.1177/0021955x05056964
53. Hoffmann B, Dietrich C, Thomann R, Friedrich C, Mülhaupt R (2000) Morphology and rheology of polystyrene nanocomposites based upon organoclay. Macromol Rapid Commun 21(1):57–61. doi:10.1002/(sici)1521-3927(20000101)21:1<57::aid-marc57>3.0.co;2-e
54. Galgali G, Ramesh C, Lele A (2001) A rheological study on the kinetics of hybrid formation in polypropylene nanocomposites. Macromolecules 34(4):852–858. doi:10.1021/ma000565f
55. Lim YT, Park OO (2001) Phase morphology and rheological behavior of polymer/layered silicate nanocomposites. Rheol Acta 40(3):220–229. doi:10.1007/s003970000126
56. Ali Mohsin ME, Arsad A, Gulrez SH, Muhamad Z, Fouad H, Alothman O (2015) Enhanced dispersion of carbon nanotubes in high density polyethylene matrix using secondary nanofiller and compatibilizer. Fibers Polym 16(1):129–137. doi:10.1007/s12221-015-0129-3
57. Nandi S, Bose S, Mitra S, Ghosh AK (2013) Dynamic rheology and morphology of HDPE-fumed silica composites: effect of interface modification. Polym Eng Sci 53(3):644–650. doi:10.1002/pen.23299
58. Jaggi H, Satapathy B, Ray A (2014) Viscoelastic properties correlations to morphological and mechanical response of HDPE/UHMWPE blends. J Polym Res 21(8):1–13. doi:10.1007/s10965-014-0482-8
59. Ezzati P, Ghasemi I, Karrabi M, Azizi H (2008) Rheological behaviour of PP/EPDM blend: the effect of compatibilization. Iran Polym J 17:669–679